Electrocatalytic reduction of oxygen at ordered mesoporous carbon functionalized with tetrathiafulvalene†

Jean Chrysostome Ndamanisha,‡ Xiangjie Bo and Liping Guo*

Received 21st September 2009, Accepted 21st December 2009
First published as an Advance Article on the web 13th January 2010
DOI: 10.1039/b919532g

A novel ordered mesoporous carbon-tetrathiafulvalene composite is synthesized. It is based on host–guest chemistry which utilizes synergic interactions between a nanostructured matrix of ordered mesoporous carbon (OMC) and the excellent electron donor properties of tetrathiafulvalene (TTF). It has been found that some interesting properties of OMC are improved. Especially the density of the edge plane-like defective sites, important groups responsible for the electrocatalytic activity towards some molecules, is increased on OMC-TTF composite. Moreover, this new material can be used to facilitate the heterogeneous electron transfer process. OMC-TTF was used, for the first time, to investigate the electrocatalytic reduction of oxygen. The results show that the electrocatalytic behavior of OMC-TTF is attributed to the unique physico-chemical properties of OMC and TTF. At the OMC-TTF modified electrode, the reduction proceeds by the direct four-electron pathway whereas at the OMC electrode the process is not direct. In order to show that the ability of OMC-TTF to promote the electron transfer can allow the application of this composite in many domains, an amperometric oxygen biosensor has been constructed based on OMC-TTF. It exhibits good response to dissolved oxygen with a large linear range and a very low detection limit. The interferences of ascorbic acid and uric acid are suppressed and the applied potential is positive enough to avoid perturbations of other electrochemically reducible compounds. The results above suggest that OMC-TTF has potential applications in the detection of dissolved oxygen and interesting properties of this composite may open up a new approach to study the electrochemical behavior of other biomolecules.

1. Introduction

Advanced materials with dimensions ranging from a few to several hundred nanometers are very important because the physicochemical properties of the nanoscopic substances can differ considerably from the properties exhibited by the same materials in the bulk.[1] Recently, nanostructured materials have attracted great interest, as they show better electrochemical performance than traditional materials.[2–5] Hence, advanced materials with nanostructures have been studied widely as electrode materials for the application of electrochemistry.[2–5]

Carbon materials have very interesting properties such as their chemical inertness, relatively wide potential window, low background current, and suitability for different types of analysis.[6,7] If they are nanostructured, they become very important. Carbon nanotubes (CNTs) belong to this group and they have been used in the preparation of modified electrodes.[4]

Besides carbon nanotubes, there has been significant interest in the development of one such novel nanostructured carbon material, *i.e.* ordered mesoporous carbon (OMC). It has been shown that, although they are both carbon materials OMCs have better electrochemical and electrocatalytic properties than those of CNTs.[8] With its well-ordered pore structure, high specific surface area and tunable pore diameters in the mesopore range,[9] OMC is suitable for applications in catalysis,[10] sensing[11] and energy storage.[12] The high density of edge plane-like defective sites (EDSs) and a large surface area on OMC may provide many favorable sites for electron transfer to compounds, which makes OMC a potential novel material for an investigation of the electrochemical behavior of substances.[13]

Moreover, the structural capabilities of OMC at the scale of a few nanometers agree with the demands of host–guest chemistry for processes involving large molecules (*e.g.*, biology and petroleum products), because zeolites or microporous materials, whose pore sizes are less than 1.2 nm, are far away from these demands.[14] Tetrathiafulvalene (TTF), a commonly artificial redox mediator[15,16] is known to mediate the electrochemistry of flavoproteins (as glucose oxidase)[17] and to facilitate different electron transfer mechanisms.[18] TTF modified carbon nanotubes have been used for bioelectrocatalytic oxidation of glucose.[19]

The determination of dissolved oxygen, particularly in aqueous solutions, is very important in chemical, physical and environmental monitoring.[20–21] Various detection systems such as fluorescence,[22] chemiluminescence,[23] and amperometric[24] methods have been developed for this purpose. The most common dissolved oxygen sensors are amperometric systems[25] and are based on the electrocatalytic reduction of oxygen.[26] One of the most important developments for a satisfactory electrocatalytic reduction of oxygen is the optimization of electrode catalysts.[27,28] There have been several reports demonstrating the

Faculty of Chemistry, Northeast Normal University, Changchun, 130024, China. E-mail: guolp078@nenu.edu.cn

† Electronic supplementary information (ESI) available: Fig. S-1 and Fig. S-2. See DOI: 10.1039/b919532g

‡ Present address: Université du Burundi, Institut de Pédagogie Appliquée, Bujumbura, 5223, Burundi.

electrocatalytic activity of both plain and modified carbon nanotube (CNTs) electrodes. The improved charge transfer for oxygen reduction at carbon nanotubes was demonstrated[29] in alkaline[30] or acidic medium.[31] Moreover, some nanoparticles have been incorporated in carbon nanotubes for the electrocatalytic reduction of oxygen.[32] However, few of these modified electrodes show the direct four-electron pathway in the oxygen reduction.[30]

Despite such potential capabilities of OMC, no report is available on the electrochemical detection of dissolved oxygen at an OMC modified electrode. Moreover, there is no reported work on the applications of OMC-based materials by host–guest synergistic interactions to promote heterogeneous electron-transfer kinetics for the electrocatalytic reduction of oxygen.

In this paper, we present a novel ordered nanocomposite based on the OMC-TTF system which utilizes remarkable and unusual host–guest synergy between an excellent electron donor of tetrathiafulvalene (TTF), and a two-dimensional (2-D) nanostructured matrix of OMC to facilitate electron-transfer processes. The OMC-TTF composite preserves the properties of an ordered mesoporous carbon and the properties are improved by the incorporation of TTF. In order to test its important properties, the reduction of oxygen is investigated. The electrocatalytic reduction of oxygen helped to understand how the characteristics of the ordered composite are interesting and attractive. A strong amperometric oxygen biosensor can be developed.

2. Results and discussion

2.1. Characterization of OMC-TTF

OMC-TTF was first examined by Fourier Transform IR (FT-IR) spectroscopy. It is clear that, from Fig. 1A, the bands around 3431, 1645, and 1523 cm^{-1} attributed to the oxygen-containing functional groups are available on OMC and OMC-TTF. This indicates that some important properties of OMC are remained after TTF incorporation. Moreover, although most of the bands in the TTF spectrum are found in the OMC spectrum, the presence of TTF in OMC-TTF is evidenced by the bands at 1071 and 1263 cm^{-1} on TTF which are shifted to 1109, 1377 cm^{-1} respectively on OMC-TTF. The relative shifts of the peaks are due to the interaction between OMC and TTF. The bands at 3431 and 1523 cm^{-1} corresponding to TTF[33] are also observed at OMC but their intensity is found to be increased at OMC-TTF. As their intensity at TTF is higher than at OMC, the increase of this intensity is an indication of the TTF incorporation because it brings more functional groups.

The surface composition of OMC-TTF was also investigated by means of X-ray photoelectron spectroscopy (XPS). Fig. 1B shows a high-resolution XPS spectrum of the S (2p) line for OMC-TTF. It can be noted that the S (2p) signal corresponding to the C–S–C bonding[34] is split into two maxima at about 163.8 eV and 164.8 eV. According to the literature,[34,35] the lower-energy line corresponds to the neutral chemical state whereas the higher binding energy is attributed to the TTF^{+} state. Both dynamical configurations TTF^{0} and TTF^{+1} can be observed with XPS because photoemission is an intrinsically rapid process.

Low angle X-ray diffraction (XRD) patterns were used to investigate the ordered structure of OMC-TTF. From Fig. 1C, it

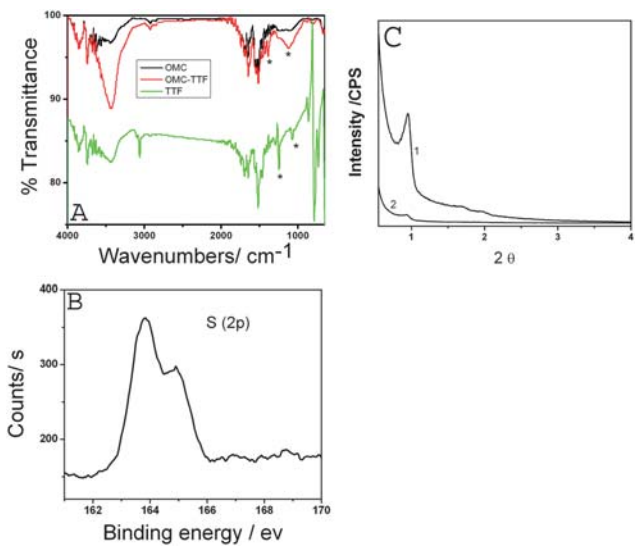

Fig. 1 FT-IR spectra of OMC, OMC-TTF and TTF, (B) high-resolution XPS spectrum of the S (2p) line for OMC-TTF, (C) small angle XRD of (A) the mesoporous materials, OMC (1) and OMC-TTF (2).

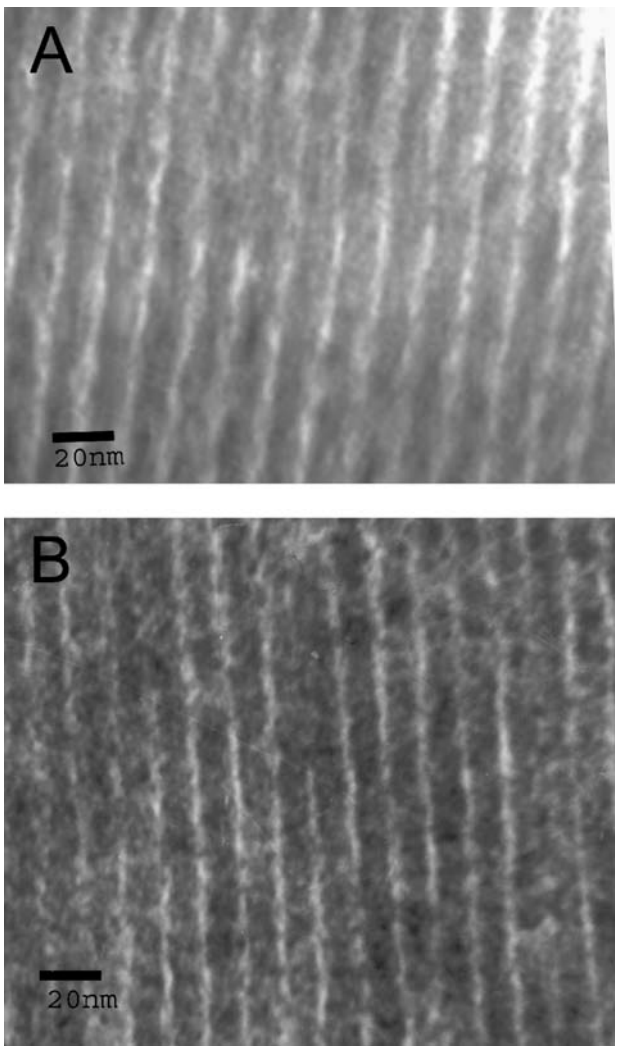

Fig. 2 TEM images of (A) OMC and (B) OMC-TTF.

can be noted that the ordered structure of OMC (curve 1) is preserved after the TTF incorporation (curve 2). Though this incorporation results in the reduced peak intensity in OMC-TTF, the ordered structure is kept. The preservation of this ordered structure is confirmed in Fig. 2A and Fig. 2B where transmission electron microscopy (TEM) images of OMC and OMC-TTF are shown. One can see that the two materials have an ordered structure, which is in agreement with the XRD results. The presence of TTF particles is indicated by the darker areas in the region of the OMC-TTF composite (Fig. 2B).

The N_2 adsorption-desorption isotherms and the Barrett–Joyner–Halenda calculations for pore size were also used and the results are shown in Fig. 3. The nitrogen sorption is essentially type IV with a clear hysteresis loop, indicating the mesoporous structure of OMC and OMC-TTF. Moreover, as shown in the insets of Fig. 3, the pore size distributions are narrow. The results indicate that the ordered mesostructure of OMC-TTF has been kept after the incorporation of the TTF.

The total surface area was found to decrease from 989 $m^2\ g^{-1}$ for OMC to 796 $m^2\ g^{-1}$ for OMC-TTF. The pore-size distributions show that the mesopore size decreases from 4.4 nm for OMC to 3.6 nm for OMC-TTF. From these results in Fig. 3, it is reasonable to conclude that OMC, having a well-defined mesoporous structure and a pore-size distribution centered at 4.4 nm, can accommodate molecules of TTF efficiently.

In our previous work[13,36] we have shown that the edge plane-like defective sites (EDSs) are very important in the electrocatalytic activity of OMC. Therefore, Raman spectroscopy was used to see whether these groups are available on OMC-TTF. As shown in Fig. 4, the Raman spectra of OMC and OMC-TTF exhibit the presence of D and G bands.[37] For OMC (Fig. 4A), D and G bands are located at 1351 cm^{-1} and 1601 cm^{-1} respectively whereas for OMC-TTF (Fig. 4B) D and G bands are observed at 1341 cm^{-1} and 1590 cm^{-1}. According to the literature,[37,38] the relative intensity ratio of the D and G bands (I_D/I_G ratio) is proportional to the number of defect sites in the graphite carbon. So the increase of I_D/I_G ratio from 0.88 for OMC to 1.54 for OMC-TTF suggests that the functionalization of OMC using TTF introduces more EDSs on the surface of OMC-TTF. The observation of the results shown above may come to a conclusion that the physico-chemical properties of OMC are preserved after incorporation of TTF in OMC-TTF. Moreover, some properties

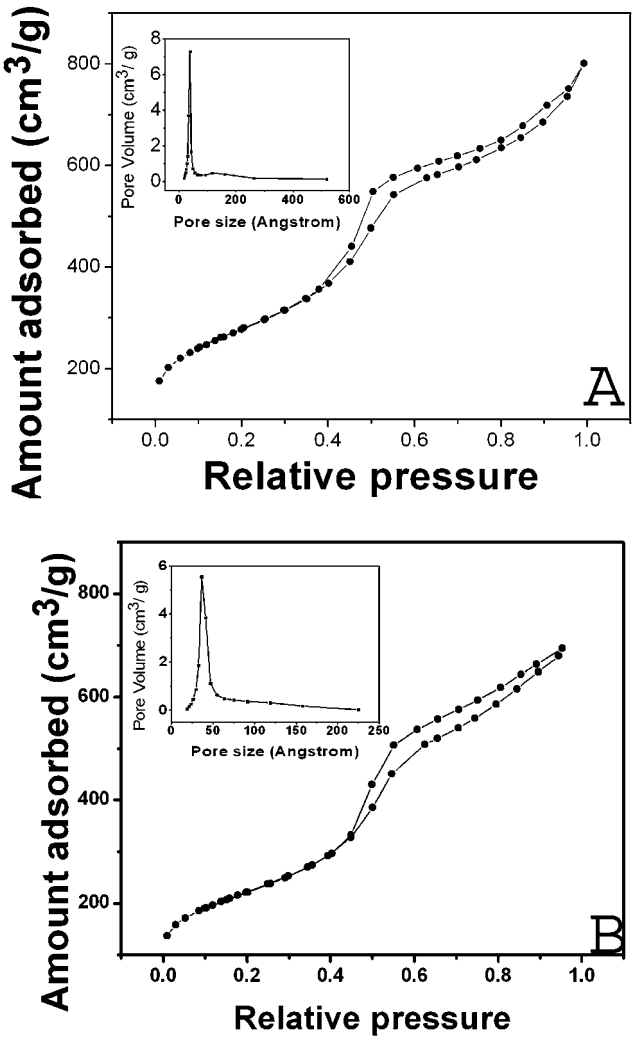

Fig. 3 Nitrogen adsorption isotherms for OMC (A) and OMC-TTF (B). Inset: Pore size distribution for OMC and OMC-TTF.

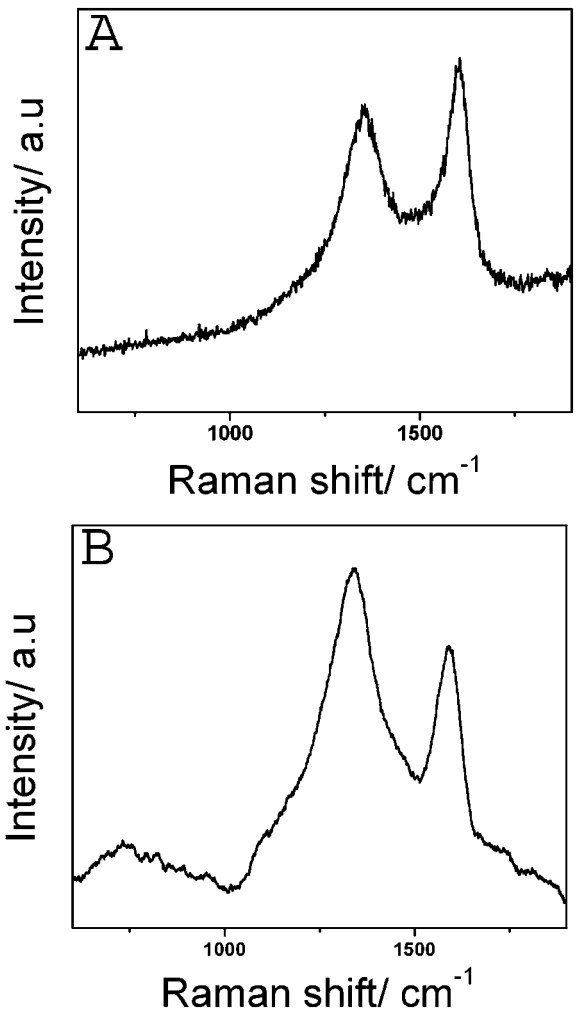

Fig. 4 Raman spectra of OMC (A) and OMC-TTF (B).

such as the increased intensity of EDSs, are even improved. This indicates that the functionalization of OMC using TTF is really important.

2.2. Electrochemical characterization

The OMC-TTF modified electrode was characterized in 10 mM $Ru(NH_3)_6Cl_3$/0.1 M KCl solution. For comparison, OMC and GC electrodes have been also characterized in the same solution. It has been found that, when the cyclic voltammograms (CVs) were recorded in the solution, the apparent voltammetric behavior (OMC and OMC-TTF) was similar to that of the GC electrode and peak currents were even smaller in some conditions. For example, the sigmoidal shape observed for the GC electrode was not obvious for the mesoporous electrodes. Also, with OMC and OMC-TTF electrodes, the increase of electrochemical signal was not obvious. This can be explained by the fast kinetics of the redox couple which reacts completely at the outermost half-pore-layer before the ions are able to diffuse into the porous system. This means that the inner porous surface is not useful in the electrochemical sense and not the complete surface area, but only the last half-pore-layer can be used for the turnover.[39] To further demonstrate this idea, the capacitance behavior was used. Fig. S-1 (supporting information) shows the cyclic voltammograms of GC, OMC and OMC-TTF electrodes in 0.5 M sulfuric acid.† For both types of porous electrodes the measured capacitance and therefore the active surface area increases dramatically on going from the GC electrode to the mesoporous electrodes. The results indicate that the electrode mesopores are highly accessible and yield an internal surface area highly larger than that of the GC electrode. The voltammetric approach proposed for porous electrodes[40] is a technique for the determination of the active surface area. One can note, from the insets of Fig. S-1,† that there is a linear dependence of the current with the scan rate and correlation coefficients of 0.999 and 0.998 for OMC and OMC-TTF electrodes are found respectively. Assuming a value of 60 μF cm^{-2} for the capacitance of unit true surface area,[40] the OMC-TTF electrode has an active surface area of 6×10^{-3} cm^2 whereas that of the OMC electrode is 7×10^{-3} cm^2. This result is in agreement with those of Fig. 3 because the pore size of OMC-TTF is smaller than that of OMC.

It has been reported that faradaic currents associated with kinetic-controlled electrochemical events are sensitive to the nanoscopic surface area of the electrode, rather than to its geometric area. Deeper and denser mesopores on an electrode surface generate larger roughness factors, that is, the ratio of nanoscopic surface area to the geometric surface area. Highly enlarged electrode areas, in nanoscale terms, boost the faradaic currents of the sluggish reaction.[41] Therefore the synthesized mesoporous electrode can be used in electrocatalysis.

Fig. 5 shows the CVs for the OMC-TTF electrode in the phosphate buffer solution (PBS) pH 7 at 50 mV s^{-1}. For comparison, CVs for the OMC and TTF electrodes are also shown in the same figure. The CV shown in Fig. 5A is the characteristics of the electrochemical behavior of OMC.[11,13] As shown in Fig. 5B, the OMC-TTF electrode exhibits two typical reversible electrochemical reactions with peaks **a** and **b**. It can be noted that the OMC electrode (Fig. 5A) shows only one reversible reaction at the potential equal to that of peak **b** in Fig. 5B,

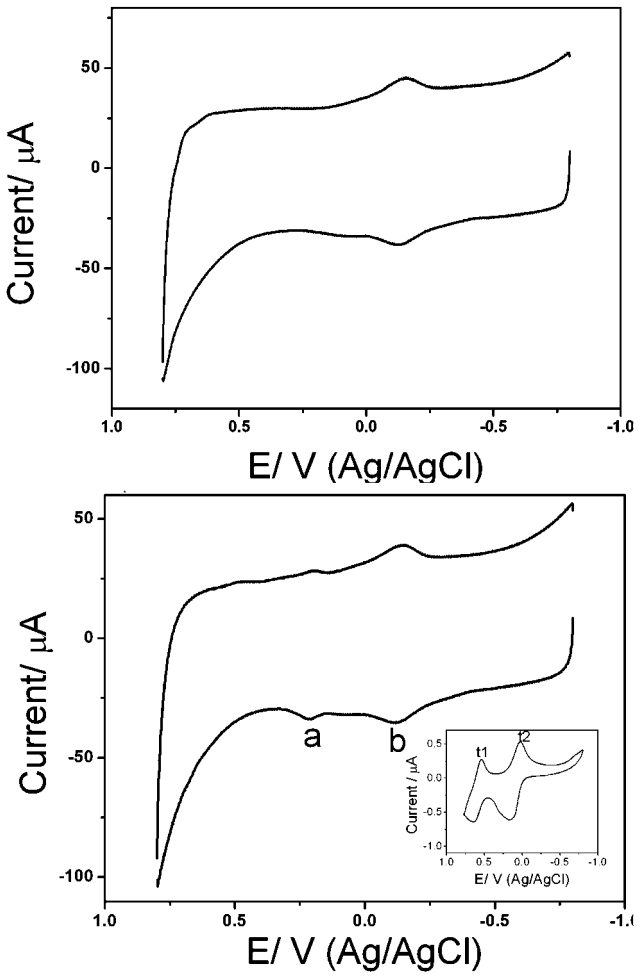

Fig. 5 Cyclic voltammograms in PBS pH 7.0 for OMC (A) and OMC-TTF (B). Scan rate 50 mV s^{-1}. The inset of (B) is the CV of TTF in the same conditions.

which indicates that the electrochemical properties due to mesoporous carbon are preserved in OMC-TTF. For the TTF electrode, the two well-defined oxidation waves corresponding to TTF[42] are observed in the inset of Fig. 5B. This indicates that, in the similar conditions, the electrochemical behavior of TTF, OMC and OMC-TTF is observed. Therefore, peak **a** in Fig. 5B is possibly attributed to the electrochemical properties of TTF in OMC-TTF. The other peak **b** may come from the contributions of OMC and TTF because peak **t2** (in TTF) is close to peak **b** in OMC-TTF. Moreover, the peaks corresponding to TTF in OMC-TTF are not obvious because of the background current of OMC.

2.3. Electrocatalytic reduction of dissolved oxygen on the OMC-TTF electrode

The OMC-TTF electrode is able to catalyze oxygen reduction in PBS pH 7.0, as shown in Fig. 6A. The solution is first degassed by bubbling nitrogen gas to record the background current–voltage curves. Under these conditions, almost no reduction current was observed in the potential range for the electrode. In contrast, after addition of a given volume of oxygen, cathodic currents

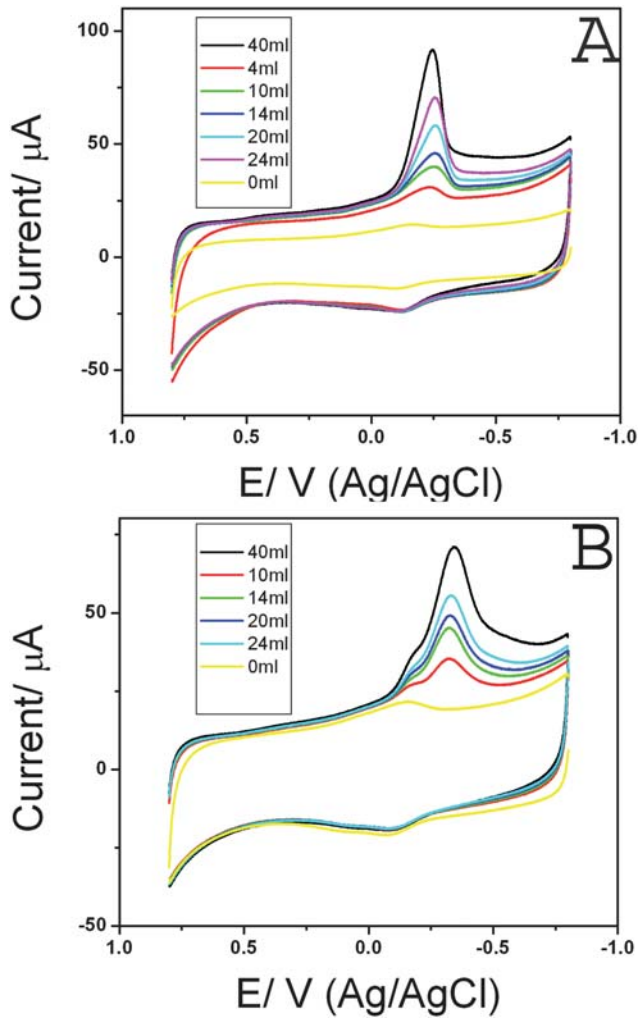

Fig. 6 Cyclic voltammograms for OMC-TTF (A) and OMC (B) electrodes recorded in PBS pH 7.0 with O_2 increasing volume added in the PBS. Scan rate 50 mV s^{-1}.

increase with increasing oxygen concentration of the solution, indicating that these peaks are associated with the reduction of oxygen. However, one can note that from Fig. 6B, the OMC electrode also possesses electrocatalytic activity towards oxygen reduction. Nevertheless, the cathodic currents are smaller than that of OMC-TTF. It is also interesting to note that there are two kinds of cathodic peaks associated with the oxygen reduction at the OMC electrode. A comparison of the cyclic voltammetric data at the two electrodes indicates that the most favorable response for oxygen reduction in terms of both potential and current is observed at the OMC-TTF electrode. It is however important to understand the effect of OMC-TTF on oxygen reduction. For the sake of this purpose, other control experiments were conducted. A GC electrode was coated with TTF and Nafion in the presence of Chitosan to obtain a TTF modified electrode. A Nafion electrode was obtained after coating GC electrode with Nafion in the presence of Chitosan. The reason of this method for the preparation of these different modified electrodes is explained in the experimental section. These modified electrodes were compared to OMC-TTF and OMC electrodes. Fig. 7A shows the results in PBS pH 7.0 at 50 mV s^{-1}. We have to keep in mind that ultrasonication has no effect on the electrocatalytic properties of OMC.[43] At the GC electrode, the CV shows a very small reduction peak current at about −0.6V and this is consistent with the literature.[44] A small reduction peak was also observed at −0.5 V for the Nafion electrode and this can be explained by the fact the conductivity of Nafion is easily lost in some conditions.[45] Alone on the GC electrode, the Nafion can be dehydrated. Nevertheless, the lowered diffusion coefficient of oxygen through the membrane can be another reason.

Another point to note is that the addition of oxygen in solution results in an increase in the peak currents at −0.17 V and −0.32 V respectively at OMC. Both peak currents increase with increasing concentrations of oxygen in the solution, indicating that the oxygen reduction undergoes two processes at the OMC electrode. The catalytic activity is evident from the obvious decrease (400 mV and 300 mV) in overpotential with a high increase in cathodic current compared to the GC electrode. The enhanced electrocatalytic activity is attributed to the edge plane-like defective sites (EDSs) on OMC.[46–48] The TTF electrode does not exhibit any cathodic peak, which suggests that it blocks the electron exchange between oxygen and the electrode. However, the OMC-TTF electrode shows a decrease of 90 mV in

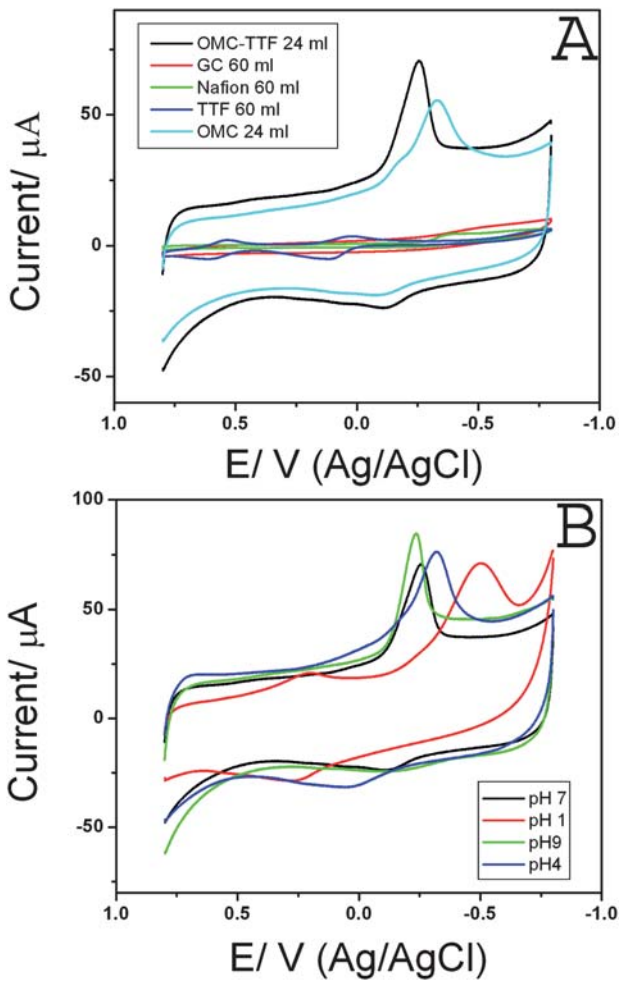

Fig. 7 Cyclic voltammograms of different electrodes in PBS pH 7.0 with different O_2 concentrations (A), and with 24 ml of O_2 at different pH for theOMC-TTF electrode (B). Scan rate: 50 mV s^{-1}.

overpotential and a current increase compared with the OMC electrode, which indicates that the presence of TTF in OMC-TTF makes the electron transfer easier. At the TTF electrode, the electron donor will repel the electrons from the electrode (at negative potential), resulting in a partially blocked electrode surface which slows the electron transfer rate.[47] Nevertheless, when TTF is incorporated in OMC-TTF, it can be regarded as an electron donor and its conjugation with OMC forms an interesting heterostructure which may play an essential role in the electron transfer like in the case of carbon nanotubes.[19]

By revisiting Fig. 6 one may find that, unlike other irreversible reactions, the oxidation of OMC and OMC-TTF did not decrease upon increasing oxygen concentrations. This is probably due to the oxidation of the oxygen-containing groups of OMC. Before the oxygen reduction, these groups are oxidized and this phenomenon is enhanced when TTF is incorporated in OMC-TTF because oxygen-containing groups are more exposed in OMC-TTF (see Fig. 1A). Fig. 7B is an indication of the influence of the pH on the oxygen reduction at the OMC-TTF electrode and it can be noted that the electrocatalytic activity of the OMC-TTF electrode towards the oxygen reduction is efficient over a wide range of pH.

To further examine the electrocatalytic reduction of oxygen, rotating disk electrode (RDE) experiments have been carried out. Fig. 8 shows the RDE voltammograms of oxygen reduction at OMC and OMC-TTF electrodes. It can be noted that the reduction current at the OMC electrode (Fig. 8A) depends slightly on the rate of the electrode rotation, indicating that the current is mainly kinetically controlled and depends for the most part on the electrochemical surface area. In order to calculate the number of electrons (n) involved in the oxygen reduction at the OMC electrode, we tried to find where the Koutecky–Levich plot is linear. We would like to mention that it was very hard to find that linear plot.

The inset of Fig. 8A shows that at −0.52 V the plot can help to calculate n according to this following relation.[7]

$$\frac{1}{I} = \frac{1}{I_k} + \frac{1}{I_d} = \frac{1}{I_k} + \frac{1}{B\omega^{1/2}}$$

$$B = 0.62nFC_oD_o^{2/3}\nu^{-1/6}$$

Where I is the measured current, I_k, I_d are the kinetic and diffusion limiting current, ω is the electrode rotation rate, n is the number of electrons, C_o is the bulk concentration of oxygen dissolved in the electrolyte, D_o is the diffusion coefficient for oxygen, F is the Faraday constant and ν is the kinematic viscosity of the electrolyte. The number of electrons can be estimated, by using the literature data for $D_o = 1.8 \times 10^{-5}$ cm^2 s^{-1},[49] and $\nu = 1.009 \times 10^{-2}$ cm^2 s^{-1},[50] and $C_o = 1.26 \times 10^{-3}$ mol L^{-1}[51] and the calculated n was close 2.

As proposed by Yeager,[52] the reduction of oxygen in aqueous solution generally proceeds by either of two pathways. One is a direct four-electron pathway through which the molecular oxygen is directly reduced to OH^- by accepting four electrons. The other is a pathway through which the molecular oxygen is reduced to HO_2^-, followed by further reduction to OH^-. There have been several reports demonstrating that the reduction of oxygen on carbon based-materials is a two-step two-electron process.[31,44] Especially the carbon nanotubes whose electrochemical behavior is quite similar to that of OMC[8] were found to show a two-electron pathway for oxygen reduction.[31,44] For the OMC electrode, it is assumed that the first reduction wave resulted from a two-electron process. Oxygen undergoes a 2e− reduction according to the reaction (1)

$$O_2 + H_2O + 2e^- \rightarrow HO_2^- + OH^- \quad (1)$$

The following reduction wave may result from the reduction of HO_2^- (Reaction 2)

$$HO_2^- + H_2O + 2e^- \rightarrow 3OH^- \quad (2)$$

At the OMC-TTF electrode (Fig. 8B), one can note that the oxygen reduction is under mixed kinetic-diffusion control. From the inset of Fig. 8B, it can be noted that the linearity of the Koutecky–Levich plot is better than in the case of the OMC electrode. Moreover, the currents at OMC-TTF are higher than those at the OMC electrode, suggesting that the functionalization of OMC with TTF is very important. The number of electrons involved in oxygen reduction was calculated to be four.

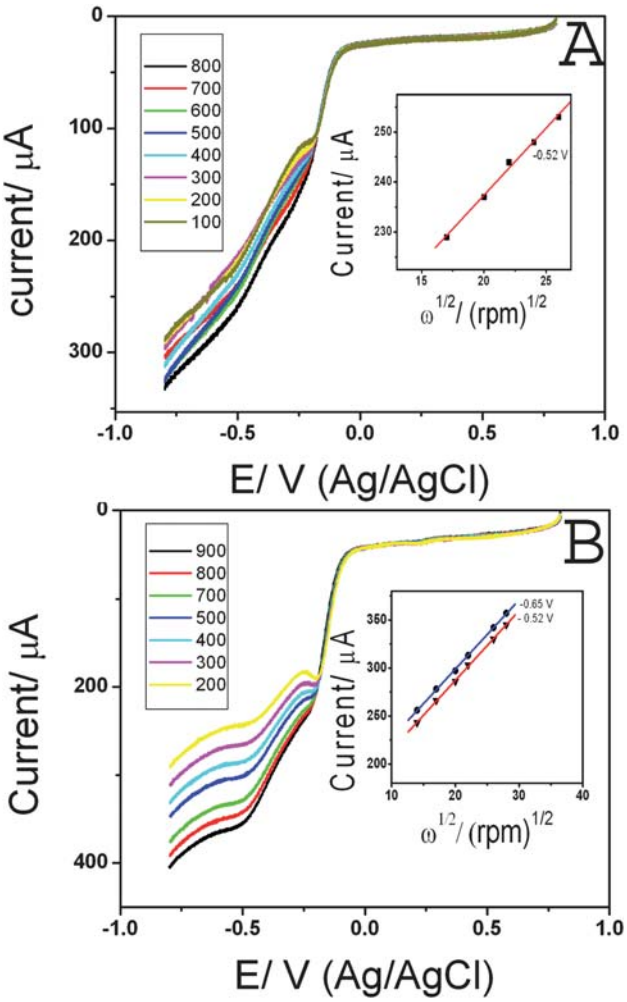

Fig. 8 (A) RDE voltammograms for OMC (A) and OMC-TTF (B) electrodes in oxygen-saturated PBS at different rotation rates (in rpm) at 50 mV s^{-1}. The insets correspond to Koutecky–Levich plots at OMC and OMC-TTF electrodes.

Therefore, the oxygen reduction undergoes only one process, suggesting that, at this electrode, the reduction proceeds by the direct four-electron pathway (Reaction 3).

$$O_2 + 2H_2O + 4e^- \rightarrow 4OH^- \quad (3)$$

The demonstrations shown above may come to the conclusion that the electrocatalytic activity for the oxygen reduction at the OMC-TTF electrode could be attributed to the unique physicochemical properties of OMC and TTF. First, the high amount of EDSs on OMC-TTF may provide many favorable sites for electron transfer to biomolecules.[13,46–48] Second, TTF is an excellent electron donor, and its conjugation with a conductive matrix of OMC forms a unique heterostructure, which may facilitate electron transfer.[19] Third, the dispersion of nanosized TTF on the nanostructured channel surface of OMC with large surface area may offer a favorable microenvironment for transferring species in solution through the pores of OMC-TTF, which would be beneficial for accelerating heterogeneous electron transfer between the electrode and species in solution.

As an example, the mechanism of the oxygen reduction at pH 7.0 has been shown above. However, it is clear that from Fig. 7B, the OMC-TTF electrode can be used to detect oxygen concentration over the pH range 1–9. This indicates not only that the modified electrode can be used in the construction of amperometric oxygen sensor but also in other domains such as industrial safety, solar cell technology or the automotive industry.[20,21]

2.4. Amperometric dissolved oxygen biosensor

As the most favorable response for oxygen reduction is observed at the OMC-TTF electrode, the amperometric sensor was developed with this electrode. In order to see whether the sensor can detect very low concentrations, oxygen saturated PBS was used. Amperometric measurements were performed in stirred PBS at an applied potential of −0.22 V. Fig. 9 shows the typical current-time responses of the OMC-TTF electrode to successive additions of oxygen saturated PBS. With the saturated concentration of 1.26×10^{-3} mol L^{-1} for dissolved oxygen,[51] an increase of current is observed after each addition of oxygen in the PBS. The response reaches 98% of the steady-state value within a few seconds. In the inset of Fig. 9, the linear dependence of the current response with the oxygen concentration (correlation coefficient 0.995) gives a range from 0.07 to 193 μM, wider than 15–45 μM of the biosensor based on VB_{12},[53] 0.06–4 μM at 2,2′-azino-bis(3-ethylbenzothiazoline-6-sulfonic acid) and laccase modified electrode[54] and 0.52–180 μM of GNP/MWNTs-FeTMAPP modified electrode.[55] The sensitivity is 0.03 μA μM^{-1} with a detection limit of 0.39 μM (S/N = 3) lower than the recently reported one.[56]

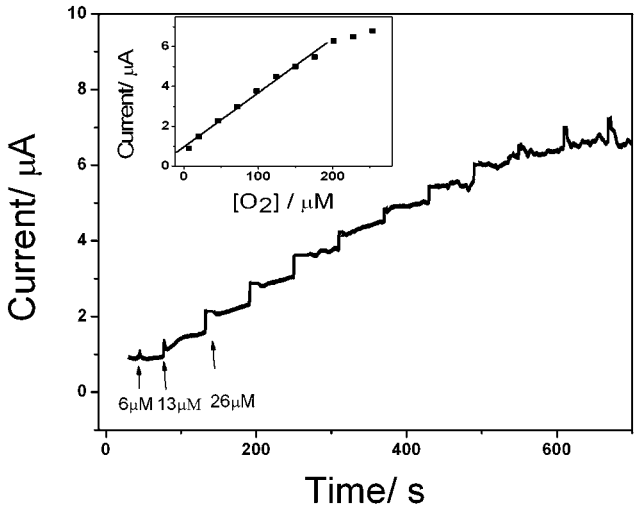

Fig. 9 Amperometric response of the OMC-TTF electrode to successive additions of oxygen-saturated PBS into stirred nitrogen-saturated PBS at −0.22 V (26 μM in the following additions). Inset: Calibration curve.

Ascorbic acid (AA) and uric acid (UA) are the common interferences.[55] Although they are not really reducible, they can disturb the detection of some substances and it is better to test their interference. As shown in Fig. S-2A,† the additions of 80 μM AA (c, d) and 26 μM UA (e) do not interfere with the amperometric response of dissolved oxygen. Moreover, the applied potential (−0.22 V) is positive enough to avoid the interference of electrochemically reducible compounds.

The reproducibility of 10 OMC-TTF electrodes was estimated by the response to 50 μM oxygen at −0.22 V. The results reveal that the sensor has satisfied reproducibility with a relative standard deviation of 5.1%. The amperometric current of dissolved oxygen remained nearly unchanged after the OMC-TTF electrode was stored at 4 °C for 1 month, indicating it could be used as a stable sensor.

In Fig. S-2B† one can note that the response to 50 μM oxygen at OMC-TTF electrode is extremely stable throughout the entire experiment with nearly unchanged current at 80 s and with 6% current diminution at 400 s with magnetic stirring.

3. Conclusions

A simple method is proposed to synthesize a novel ordered mesoporous carbon- tetrathiafulvalene composite with interesting properties. The good mechanical stability, high specific surface area, and high density of EDSs of OMC, and the unique electronic structure of TTF, facilitate the manipulation of OMC-TTF for applications. The electrocatalytic reduction of oxygen helped to show the important characteristics of the ordered composite. The synergy of OMC and TTF enhances the electrocatalytic activity of the new material towards the reduction of dissolved oxygen. The enhanced electrocatalytic activity towards oxygen would provide a potential application of the composite for preparing an oxygen biosensor. This result is an indication that, with its important characteristics, OMC-TTF can be used to detect other biomolecules on the basis of the electrocatalysis of OMC and TTF. Electrochemical behaviors of some biocompounds are being investigated. This research may open up a new challenge and approach to explore the properties of OMC-TTF derivatives hybrid materials for the potential applications of electrofunctional devices.

4. Experimental

Reagents. Nafion solution (5% wt in 15–20% water/lower aliphatic alcohols) and tetrathiafulvalene (TTF) were obtained from Aldrich. Chitosan was from Zhejiang Jinqiao Biochemicals

Company (China). All other chemicals were of analytical reagent grade and were used as received. Double distilled water was used to prepare aqueous solutions. The 0.1 M phosphate buffer solution (PBS), which was made up from Na_2HPO_4, NaH_2PO_4, and H_3PO_4, was employed as a supporting electrolyte.

Synthesis of OMC and OMC-TTF. The mesoporous Santa Barbara No15 (SBA- 15) was prepared using Pluronic P123 (non-ionic triblock copolymer EO20PO70EO20) as a surfactant and tetraethoxysilane as a silica source, according to the literature.[57] OMC was synthesized using SBA-15 as a template, sucrose as carbon source following the reported procedure.[58]

The procedure of immobilizing TTF on the channel surface of OMC was as follows: First, 50 mg of OMC and 35 mg of TTF were dispersed in 40 mL of ethanol. Second, the mixture was subjected to ultrasound at room temperature for 3 h. During irradiation, water flow was utilized to cool the glass vessel in the bath. After filtration, the reaction mixture was washed with a large excess of ethanol and double distilled water. As a final step, the remaining solid (denoted as OMC-TTF) was dried in a vacuum oven at 60 °C overnight.

Preparation of modified electrodes. The glassy carbon (GC) electrode was polished before each experiment with 1, 0.3 and 0.05 μm alumina powder, respectively. It was rinsed thoroughly with doubly distilled water between each polishing step. Then it was washed successively with a diluted solution of nitric acid + acetone (V : V = 1 : 1) and doubly distilled water in ultrasonic bath and dried in air. 10 mg of OMC-TTF were added to 9 ml water. Many papers have reported the size exclusion effect of Chitosan membrane for biosensor applications.[59–61] Moreover, it has been found that OMC can be suspended in a solution of Nafion and this ability of Nafion to disperse OMC results in the construction of an amperometric epinephrine sensor.[62] Therefore, Chitosan and Nafion were both used in this work. After addition of 1 ml of Nafion and 1 ml of Chitosan 1%, the mixture was sonicated for 30 min. The colloid (10 μl) was dropped on the surface of the GC electrode and this was allowed to dry at room temperature. The obtained modified electrode was denoted as OMC-TTF electrode. For the control experiments, OMC and Nafion electrodes were prepared in the same way, with Chitosan for each electrode. The TTF electrode was prepared with ethanol instead of water.

Electrochemical and other measurements. Electrochemical experiments were carried out using a CHI 830b Electrochemical Analyzer (Chenhua Instruments, Shanghai) in a conventional three-electrode cell. The working electrode used was glassy carbon (GC) electrode or the modified electrode. A platinum electrode was taken as the counter electrode and an Ag/AgCl (in saturated KCl solution) electrode served as the reference electrode. Rotating disk electrode (RDE) experiments were performed on a PARSTAT 2273 potentiostat with a model 616 Disk electrode. The sample solutions were purged with purified nitrogen for at least 20 min to remove oxygen prior to the beginning of a series of experiments. For the oxygen reduction, a given volume of oxygen at atmospheric pressure and room temperature was introduced in the oxygen-free phosphate buffer solution (PBS) pH 7.0. In the amperometric determination, the PBS was saturated with the pure nitrogen in the three-electrode cell (in order to remove the oxygen in the solution). The oxygen-saturated PBS was then added into the nitrogen-saturated PBS. Small angle X-ray diffraction (XRD) patterns were obtained on an X-ray Pmax 2200 PC (Rikagu, Japan) operating at 40 kV and 40 mA and using CuKα radiation. Transmission electron microscopy (TEM) images were obtained on a JEOL JEM-2010 electron microscope. Infrared spectrum of the sample was recorded with Nicolet Magna 560 FT-IR Spectrometer with KBr plate in the 400–4000 cm^{-1} region. XPS scans of samples were taken using Thermo ESCA LAB spectrometer (USA) and Fe_3O_4 was used as a reference. Nitrogen adsorption and desorption isotherms were measured on ASAP2020 (Micromeritics, USA). The pore size distributions (PSD) were calculated by the Barrett–Joyner–Halenda (BJH) method. Raman spectroscopy was done with Renishaw-1000 Raman spectrometer Instrument (Renishaw, UK).

Acknowledgements

The authors gratefully acknowledge the financial support by the National Natural Science Foundation of China (No. 20875012), and Analysis and Testing Foundation of Northeast Normal University.

References

1 C. N. R. Rao, G. U. Kulkarni, P. John Thomas and P. P. Edwards, *Chem.–Eur. J.*, 2002, **8**, 28.
2 L. Wu, X. Zhang and H. Ju, *Anal. Chem.*, 2007, **79**, 453.
3 M. Musameh, J. Wang, A. Merkoci and Y. Lin, *Electrochem. Commun.*, 2002, **4**, 743.
4 J. Wang, *Electroanalysis*, 2005, **17**, 7.
5 A. Walcarius, *C.R. Chim.*, 2005, **8**, 693.
6 R. L. McCreery, In *Electroanalytical Chemistry*; Bard, A. J., Ed.; John Wiley and Sons: New York, 1991; Vol. 17, pp 221–374.
7 A. J. Bard, L. R. Faulkner, *Electrochemical methods* 2nd ed. Wiley, New York 2001.
8 M. Zhou, L. Shang, B. Li, L. Huang and S. Dong, *Electrochem. Commun.*, 2008, **10**, 859.
9 R. Ryoo, S. H. Joo and S. Jun, *J. Phys. Chem. B*, 1999, **103**, 7743.
10 S. H. Joo, S. J. Choi, I. Oh, J. Kwak, Z. Liu, O. Terasaki and R. Ryoo, *Nature*, 2001, **412**, 169.
11 (*a*) J. C. Ndamanisha and L. P. Guo, *Biosens. Bioelectron.*, 2008, **23**, 1680; (*b*) J. C. Ndamanisha, L. P. Guo and G. Wang, *Microporous Mesoporous Mater.*, 2008, **113**, 114.
12 M. Hartmann, *Chem. Mater.*, 2005, **17**, 4577.
13 M. Zhou, J. Ding, L. P. Guo and Q. K. Shang, *Anal. Chem.*, 2007, **79**, 5328.
14 D. R. Rolison, *Chem. Rev.*, 1990, **90**, 867–878.
15 F. Palmisano, P. G. Zamnbonin, D. Centone and M. Quinto, *Anal. Chem.*, 2002, **74**, 5913.
16 S. Campuzano, R. Galvez, M. Pedrero, F. J. M. de Villena and J. M. Pingarron, *Anal. Bioanal. Chem.*, 2003, **377**, 600.
17 Y. Sekine and E. A. H. Hall, *Biosens. Bioelectron.*, 1998, **13**, 995.
18 G. F. Khan, M. Ohwa and W. Wernet, *Anal. Chem.*, 1996, **68**, 2939.
19 B. Kowalewska and P. J. Kulesza, *Electroanalysis*, 2009, **21**, 351.
20 J. R. Stetter and J. Li, *Chem. Rev.*, 2008, **108**, 352.
21 R. T. Bailey, F. R. Cruickshank, G. Deans, R. N. Gillanders and M. C. Tedford, *Anal. Chim. Acta*, 2003, **487**, 101.
22 T. M. Freeman and W. R. Seitz, *Anal. Chem.*, 1981, **53**, 98.
23 P. Westbroek and E. Temmerman, *Anal. Chim. Acta*, 2001, **437**, 95.
24 H. S. Liu, L. Zhang, J. J. Zhang, D. Ghosh, J. Jung, B. W. Downing and E. Whittemore, *J. Power Sources*, 2006, **161**, 743.
25 M. L. Hichman, *The Measurement of Dissolved Oxygen*; John Wiley: New York, 1978.
26 R. Knake, P. Jacquinot, A. W. E. Hodgson and P. C. Houser, *Anal. Chim. Acta*, 2005, **549**, 1.
27 J. Prakash and H. Joachin, *Electrochim. Acta*, 2000, **45**, 2289.
28 U. A. Paulus, T. J. Schmidt, H. A. Gasteiger and R. J. Behm, *J. Electroanal. Chem.*, 2001, **495**, 134.

29 P. J. Britto, K. S. V. Santhanam, A. Rubio, J. A. Alonso and P. M. Ajayan, *Adv. Mater.*, 1999, **11**, 154.
30 Y. Shen, J. Liu, A. Wu, J. Jiang, L. Bi, B. Liu, Z. Li and S. Dong, *Langmuir*, 2003, **19**, 5397.
31 Y. Lin, X. Cui and X. Ye, *Electrochem. Commun.*, 2005, **7**, 267.
32 A. Kongkanand, S. Kuwabata, G. Girishkumar and P. Kamat, *Langmuir*, 2006, **22**, 2392.
33 (*a*) R. Bozio, I. Zanon, A. Girlando and C. Pecile, *J. Chem. Phys.*, 1979, **71**, 2282; (*b*) J. C. Goeltz and C. P. Kubiak, *J. Phys. Chem. C*, 2008, **112**, 8114.
34 I. Malfant, K. Rivasseau, J. Fraxedas, C. Faulmann, D. Caro, L. Lydie Valade, L. Kaboub, J. M. Fabre and F. Senocq, *J. Am. Chem. Soc.*, 2006, **128**, 5612.
35 M. Sing, U. Schwingenschlogl, R. Claessen and C. S. Jacobsen, *Phys. Rev. B*, 2003, **67**, 125402.
36 J. C. Ndamanisha, J. Bai, B. Qi and L. P. Guo, *Anal. Biochem.*, 2009, **386**, 79.
37 V. Georgakilas, D. Voulgaris, E. Vazquez, M. Prato, D. M. Guldi, A. Kukovecz and H. Kuzmany, *J. Am. Chem. Soc.*, 2002, **124**, 14318.
38 A. C. Ferrari and J. Robertson, *Phys. Rev. B*, 2000, **61**, 14095.
39 R. Szamocki, A. Velichko, C. Holzapfel, F. Mucklich, S. Ravaine, P. Garrigue, N. Sojic, R. Hempelmann and A. Kuhn, *Anal. Chem.*, 2007, **79**, 533.
40 S. Trasatti and O. A. Petrii, *Pure Appl. Chem.*, 1991, **63**, 711.
41 S. Park, T. D. Chung and H. C. Kim, *Anal. Chem.*, 2003, **75**, 3046.
42 K.-N. Kuo, J. R. Lenhard, D. C. Green and R. W. Murray, *Anal. Chem.*, 1979, **51**, 745.
43 M. Zhou, J. Guo and L. P. Guo, *Anal. Chem.*, 2008, **80**, 4642.
44 P. Gajendran and R. Saraswath, *J. Phys. Chem. C*, 2007, **111**, 11320.
45 H. L. Tang and M. Pan, *J. Phys. Chem. C*, 2008, **112**, 11556.
46 C. E. Banks and R. G. Compton, *Analyst*, 2005, **130**, 1232.
47 C. E. Banks, R. R. Moore, T. J. Davies and R. G. Compton, *Chem. Commun.*, 2004, **16**, 1804.
48 C. E. Banks, T. J. Davies, G. G. Wildgoose and R. G. Compton, *Chem. Commun.*, 2005, 829.
49 N. Alexeyeva, T. Loaksonen, K. Kontturi, F. Mirkhalaf, D. J. Schiffrin and K. Tammeveski, *Electrochem. Commun.*, 2006, **8**, 1475.
50 N. M. Markovic, H. A. Gasteiger, B. N. Grgur and P. N. Ross, *J. Electroanal. Chem.*, 1999, **467**, 157.
51 A. Schumpe, I. Adler and W. D. Deckwer, *Biotechnol. Bioeng.*, 1978, **20**, 145.
52 E. Yeager, *J. Mol. Catal.*, 1986, **38**, 5.
53 M. S. Lin, H. J. Leu and C. H. Lai, *Anal. Chim. Acta*, 2006, **561**, 164.
54 C. Mousty, L. Vieille and S. Cosnier, *Biosens. Bioelectron.*, 2007, **22**, 1733.
55 Y. Liu, Y.-L. Yan, J. Lei, F. Wu and H. Ju, *Electrochem. Commun.*, 2007, **9**, 2564.
56 L. Hutton, M. E. Newton, P. R. Unwin and J. V. Macpherson, *Anal. Chem.*, 2009, **81**, 1023.
57 D. Zhao, Q. Huo, J. Feng, B. F. Chmelka and G. D. Stucky, *J. Am. Chem. Soc.*, 1998, **120**, 6024.
58 S. Jun, S. H. Joo, R. Ryoo, M. Kruk, M. Jaroniec, Z. Liu, T. Ohsuna and O. Terasaki, *J. Am. Chem. Soc.*, 2000, **122**, 10712.
59 M. Yang, Y. Yang, B. Liu, G. Shen and R. Yu, *Sens. Actuators, B*, 2004, **101**, 269.
60 X. Wei, J. Cruz and W. Gorski, *Anal. Chem.*, 2002, **74**, 5039.
61 J. Cruz, M. Kawasaki and W. Gorski, *Anal. Chem.*, 2000, **72**, 680.
62 M. Zhou, L. P. Guo, Y. Hou and X. J. Peng, *Electrochim. Acta*, 2008, **53**, 4176.